

Overall retrieval error budget and a posteriori justification of modeling choices

G.P. Stiller

Abstract: In this paper we present the assessment of individual forward model errors by disregarding a number of atmospheric properties and processes KOPRA is able to handle with, as well as an over-all error budget with respect to these parameters. We demonstrate that a number of specific features of KOPRA are capable to improve the retrieval accuracy in MIPAS/ENVISAT data analysis compared to approaches which neglect the modeling of these atmospheric and/or instrumental properties.

1 Introduction

KOPRA has been designed to allow modeling of a number of atmospheric properties and processes relevant for the altitude range the MIPAS mission will cover, as well as the instrument specific details of MIPAS itself. Although we decided to cover all these aspects, we are aware that some of them may be disregarded in one or the other situation of data analysis without too serious loss of accuracy. However, in order not to rely on *ad hoc* decisions and introduce retrieval errors due to simplified assumptions, a study has been performed to quantify the relevance of these effects. We have assessed the forward modeling error and its mapping on the retrieval error for a number of KOPRA specific features like modeling of the Earth's oblateness, temperature and vmr horizontal inhomogeneities, neglection of NLTE effects and line-mixing, insufficient modeling of MIPAS' field of view and instrumental line shape, and others. Based on this study, *a posteriori* decisions on the relevance of these effects and thus on the possibility to simplify the retrieval cases, have become possible.

2 Modeling error related to raytracing in a non-spherical atmosphere

In contrast to most other radiative transfer models, KOPRA makes use of the approach of differential displacement of the ray path[1] which assumes linear variation of the refractive index within each incremental step of integration. Contrary to the implementation of Snell's Law for spherical media, this approach can easily be extended for application to an ellipsoidal earth shape. For our implementation, the WGS84 reference ellipsoid has been used. It was shown that the spherical approximation of the earth, making use of the local curvature of the WGS84 reference ellipsoid, is sufficient as long as measurement geometry is characterized by the observer altitude and the tangent altitude (see Part IV: 'Atmospheric raypath modeling for radiative transfer algorithms' and Table 1). However, earth shape considerations may be of major importance if the measurement geometry is characterized by the observer altitude and the elevation angle of the measurement. This is in particular true if the tangent point is a fit parameter rather than a constant, and the latitude of the tangent point is changing from iteration to iteration of a pointing retrieval. This is illustrated by Table 2.

Table 1: Path lengths and CO₂ column amounts as calculated by KOPRA using the WGS84 reference ellipsoid, for spherical earth, and assuming local curvature radius of the WGS84 reference ellipsoid. Calculations were made for various observer positions and viewing directions (azimuth = 0° means pointing southward), and for 8 km tangent height. The tangent height is assumed to be known.

	Latitude[°]/ Azimuth[°]	0/0	0/90	45/0	90/0
Path length [km]	WGS 84	2446.6	2455.0	2452.8	2459.1
	Spherical	2452.8	2452.8	2452.8	2452.8
	Spherical, curvature radius of WGS 84 at tangent point	2446.4	2455.0	2452.8	2459.2
CO ₂ [10 ²³ molec/cm ²]	WGS 84	2.3051	2.3135	2.3113	2.3177
	Spherical	2.3114	2.3114	2.3114	2.3114
	Spherical, curvature radius of WGS 84 at tangent point	2.3051	2.3135	2.3114	2.3178

We conclude from this comparison that for the application as planned, namely the retrieval of elevation angles from measured spectra for various geolocations, and the modeling of the earth's ellipticity is mandatory.

Table 2: Path lengths, CO₂ column amounts, and tangent heights as calculated by KOPRA using the WGS84 reference ellipsoid, and for spherical earth. Calculations were made for various observer positions and viewing directions (azimuth = 0° means pointing southward). Observer altitude is 800 km, nadir angle is 62.7675°

	Latitude[°]/ Azimuth[°]	0/0	0/90	45/0	90/0
Path length [km]	WGS 84	2449.3	2541.6	2487.7	2424.0
	Spherical	2514.6	2514.6	2514.6	2514.6
CO ₂ [10 ²³ molec/cm ²]	WGS 84	2.3101	4.3490	3.1580	4.3020
	Spherical	3.6880	3.6880	3.6880	3.6880
Tangent height [km]	WGS 84	7.992	2.914	5.537	0.922
	Spherical	4.290	4.290	4.290	4.290

3 Mapping of radiative transfer modeling errors on the retrieval error of trace species

3.1 Method

In the following we present the estimation of the mapping of radiative transfer modeling errors on the retrieval of target species, the comparison to the random retrieval error due to measurement noise, and the assessment of the expected overall retrieval error which results from these individual uncertainties. For estimation of retrieval errors we follow the scheme proposed by Ref. [2] who apply linear theory which usually is considered sufficient for error propagation problems in this context[3]. The mapping of measurement noise, represented by the measurement covariance matrix \mathbf{S}_y , on the retrieval, represented by the retrieval covariance matrix \mathbf{S}_x is estimated as

$$\mathbf{S}_x = (\mathbf{K}^T \mathbf{K})^{-1} \mathbf{K}^T \mathbf{S}_y \mathbf{K} (\mathbf{K}^T \mathbf{K})^{-1} \quad (1)$$

where \mathbf{K} is the Jacobian matrix, evaluated as reported by Ref. [4]. The Jacobian matrix contains the derivatives of the spectral signal with respect to the fit parameters. τ denotes a transposed matrix.

Model errors and parameter errors are characterized by correlations in the spectral domain. The retrieval errors $\Delta x_{i,j}$ of the fit parameter x_i due to error source j are approximated linearly

$$\Delta X_j = \begin{pmatrix} \Delta x_{1,j} \\ \Delta x_{2,j} \\ \vdots \\ \Delta x_{i_{max},j} \end{pmatrix} = (\mathbf{K}^T \mathbf{K})^{-1} \mathbf{K}^T (Y_{error,j} - Y_{true}). \quad (2)$$

Y_{true} is a synthetic spectrum modeled with KOPRA including all available physics, while $Y_{error,j}$ is a spectrum calculated under neglect of physical effect j .

The total retrieval error Δx_i of the target quantity x_i then is calculated as

$$\Delta x_i = \sqrt{\sigma_i^2 + \left(\sum_{l=1}^{l_{max}} \Delta x_{i,l} \right)^2 + \sum_{j=1}^{j_{max}} (\Delta x_{i,j})^2} \quad (3)$$

where σ_i^2 is the i^{th} diagonal element of \mathbf{S}_x . Errors labeled l are assumed correlated among each other and therefore are added linearly while errors labeled j are assumed uncorrelated among each other and therefore are added quadratically.

3.2 Case Studies

In order to demonstrate the impact of disregarding atmospheric and radiative properties on the spectrum and the related retrieval error we performed a number of case studies. The spectral ranges selected for the case studies are somewhat arbitrary, as they do not all represent optimized so-called microwindows for the analysis of MIPAS data. They were selected as they appeared to be suitable to demonstrate the effects under investigation. Dedicated studies for selection of optimized microwindows for the MIPAS experiments are underway and are beyond the scope of this study[5]. In all cases we generated a "perfect" reference spectrum including all effects considered to be relevant for the correct modeling of the radiance (Y_{true} in Eq. 2). The Jacobians were provided simultaneously with the forward calculation as described in Ref [4]. Besides the target species, an empirical background continuum radiation was an additional fit parameter. A number of less perfect "approximation" spectra were generated, each of them excluding one of the effects under investigation ($Y_{error,j}$ in Eq. 2).

Effects under investigation were line mixing, NLTE, horizontal inhomogeneities of temperature, pressure, and volume mixing ratio (vmr) profiles of target and interfering species, isotopic abundance profiles deviating from the altitude-constant values used in the HITRAN compilation, and the MIPAS specific FOV and ILS modeling. The apodized noise levels assumed were 3.035×10^{-8} W/(cm² sr cm⁻¹) and 2.549×10^{-9} W/(cm² sr cm⁻¹) for the filter ranges A (685-970 cm⁻¹) and D (1820-2410 cm⁻¹), respectively, according to predictions as provided by ESA[6]. The resulting individual errors and the total error of the retrieved target quantity then were estimated by application of the method outlined above. For the evaluation of the total error, errors due to neglect of NLTE and line-mixing and improper FOV and ILS modeling have been considered correlated, and therefore added linearly, while errors due to horizontal inhomogeneities and isotopic abundances have been considered uncorrelated.

All reference spectra were modeled for the 1976 US Standard atmosphere[7], and trace gas abundance vertical profiles were provided by Echle et al.[8]. The vibrational temperature profiles were from Kerridge and coworkers for O₃, and López-Puertas and coworkers (H₂O, CO₂, and N₂O), both as reported in Ref. [5]. For NO, vibrational temperature profiles from Ref. [9] were used. Profiles of volume

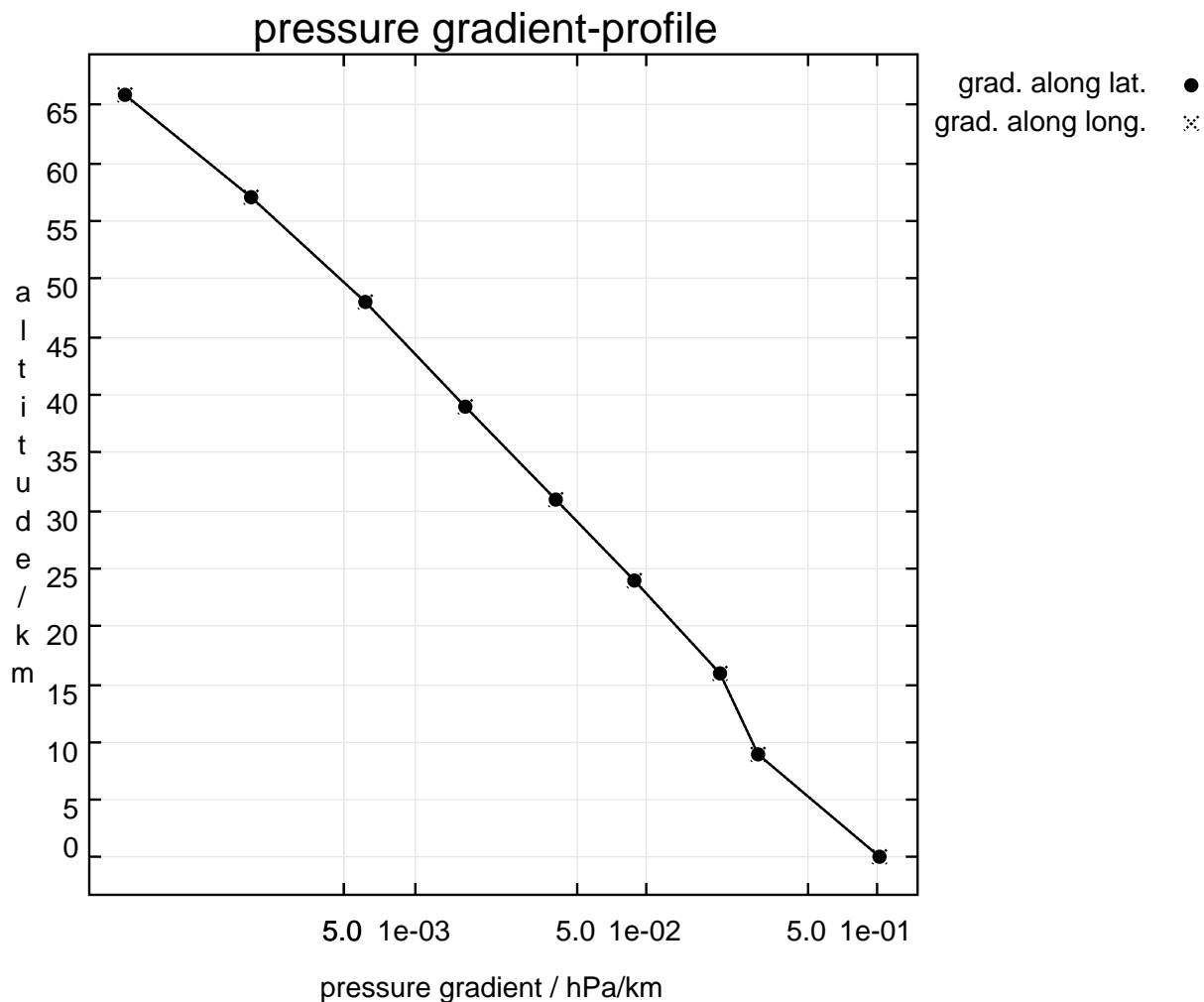


Figure 1: Horizontal inhomogeneities for pressure

mixing ratio gradients were used as estimates of maximum values to be measured by MIPAS[10].

We considered horizontal inhomogeneities for pressure (see Fig. 1), temperature (3 K/ 100 km for all altitudes), and H₂O, O₃, HNO₃, ClONO₂, and NO₂ (see Figs. 2 to 6).

Dedicated vertical profiles for isotopomeric abundances were compiled from the literature for water vapor[11] and ozone[12].

For the approximation spectra, line-mixing, NLTE, and horizontal inhomogeneities were disregarded. Instead of the isotopomeric profiles above, the altitude-constant HITRAN standard values were used. The ILS was modeled for a circular FOV and assuming perfect performance of the instrument (no modulation loss, no phase error). Instead of integration over the FOV, only radiance along the center beam was modeled.

Results of the retrieval error assessment are presented in Table 3.

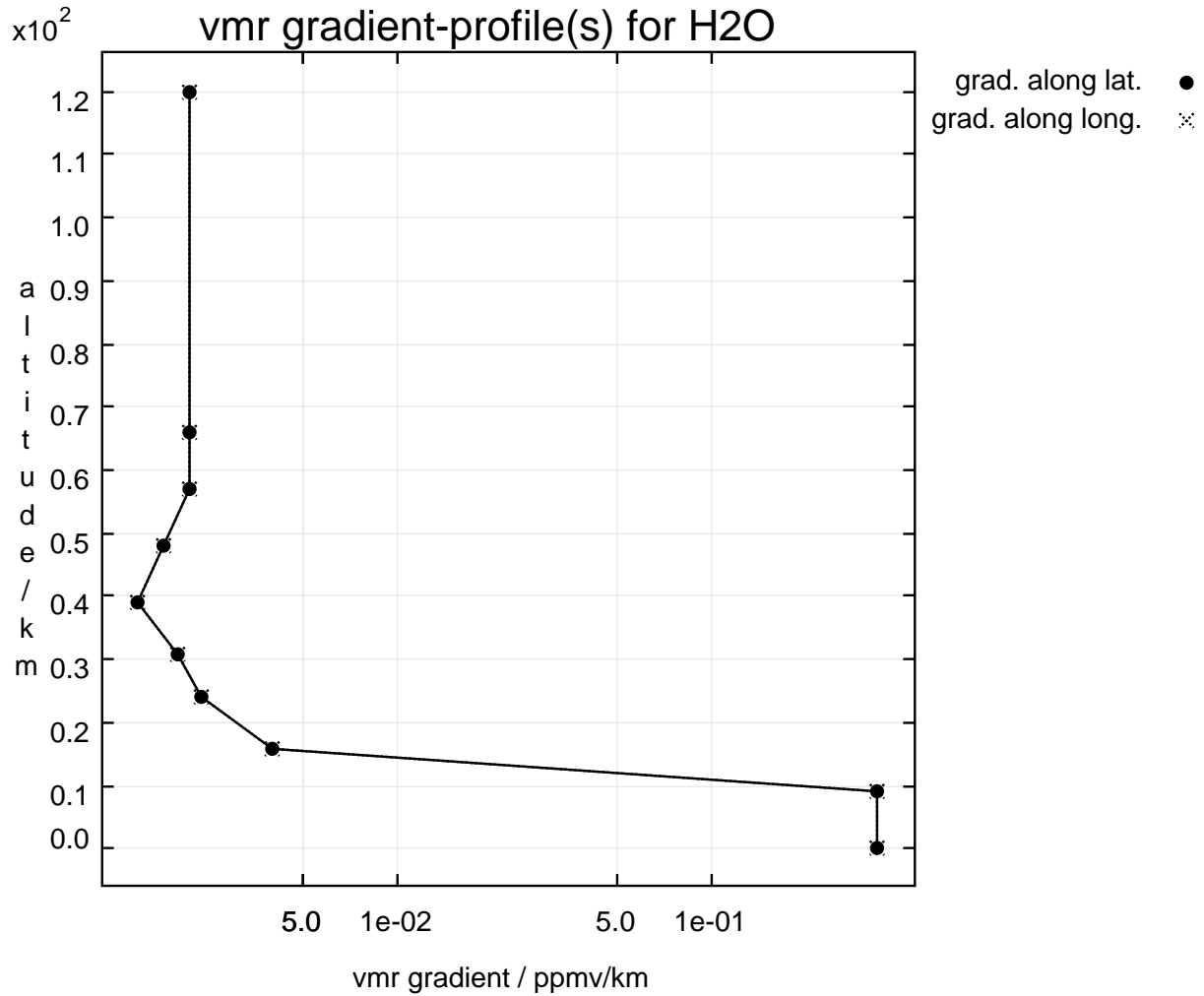
Figure 2: Horizontal inhomogeneities for H₂O

Table 3: Results of test cases: relative retrieval errors

Source of error	790.0-800.0 cm ⁻¹	1861.3-1861.9 cm ⁻¹	870.875-871.975 cm ⁻¹
Target species, tangent altitude	CCl ₄ , 8km	H ₂ O, 50 km	HNO ₃ , 22 km
Noise	2.6 %	35.7 %	6.7 %
Grad T	11.0 %	-3.7 %	1.8 %
Grad vmr	8.2 %	/	-3.9 %
Grad p	-0.06 %	-2.9 %	-2.5 %
Isotopic abundances	/	0.2 %	/
NLTE	-5.8 %	3.4 %	/
Line mixing	-42.3 %	0	/
ILS	0.2 %	3.0 %	2.6 %
FOV	-42.6 %	0.3 %	3.0 %
Total	91.6 %	36.6 %	8.9 %

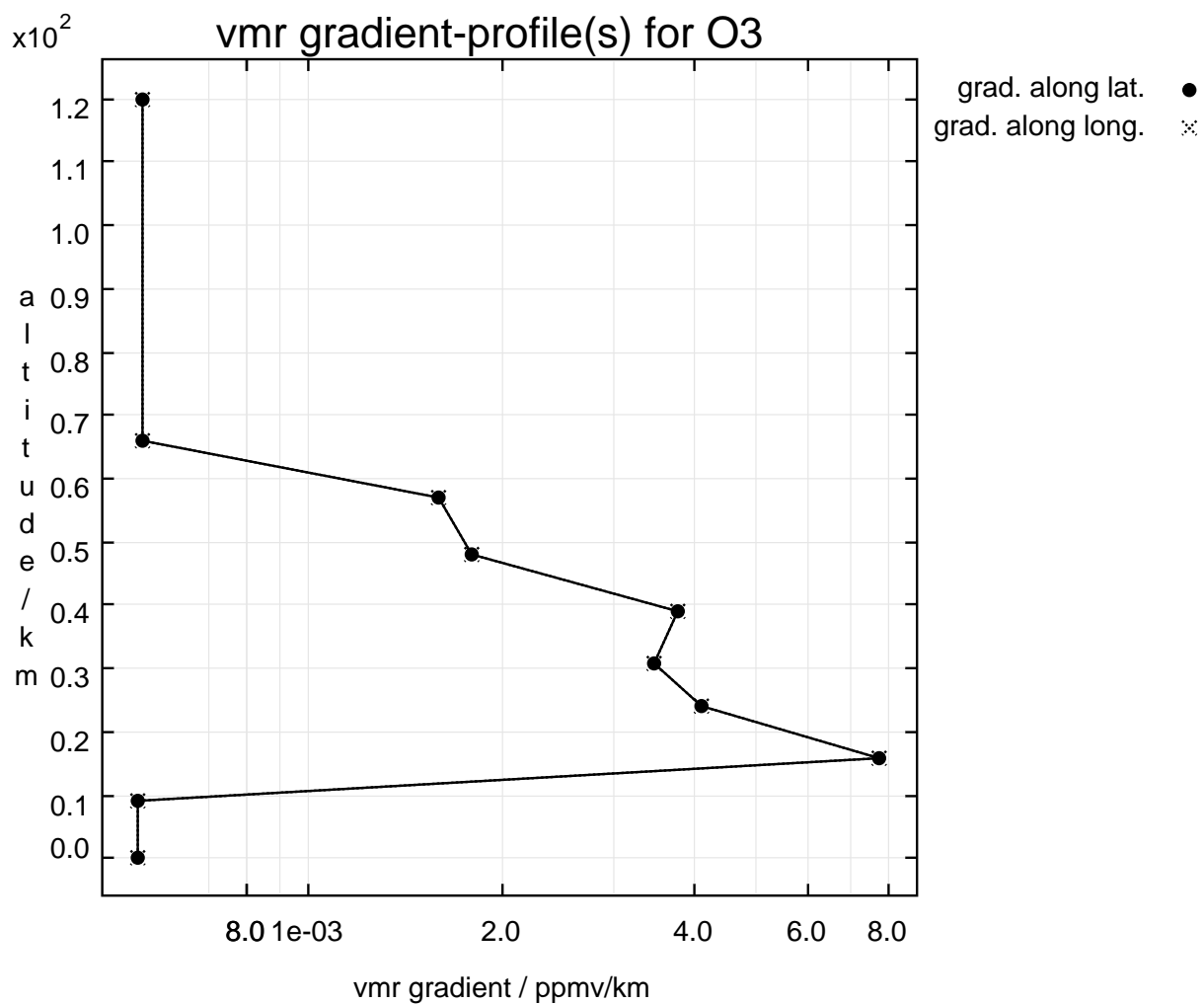
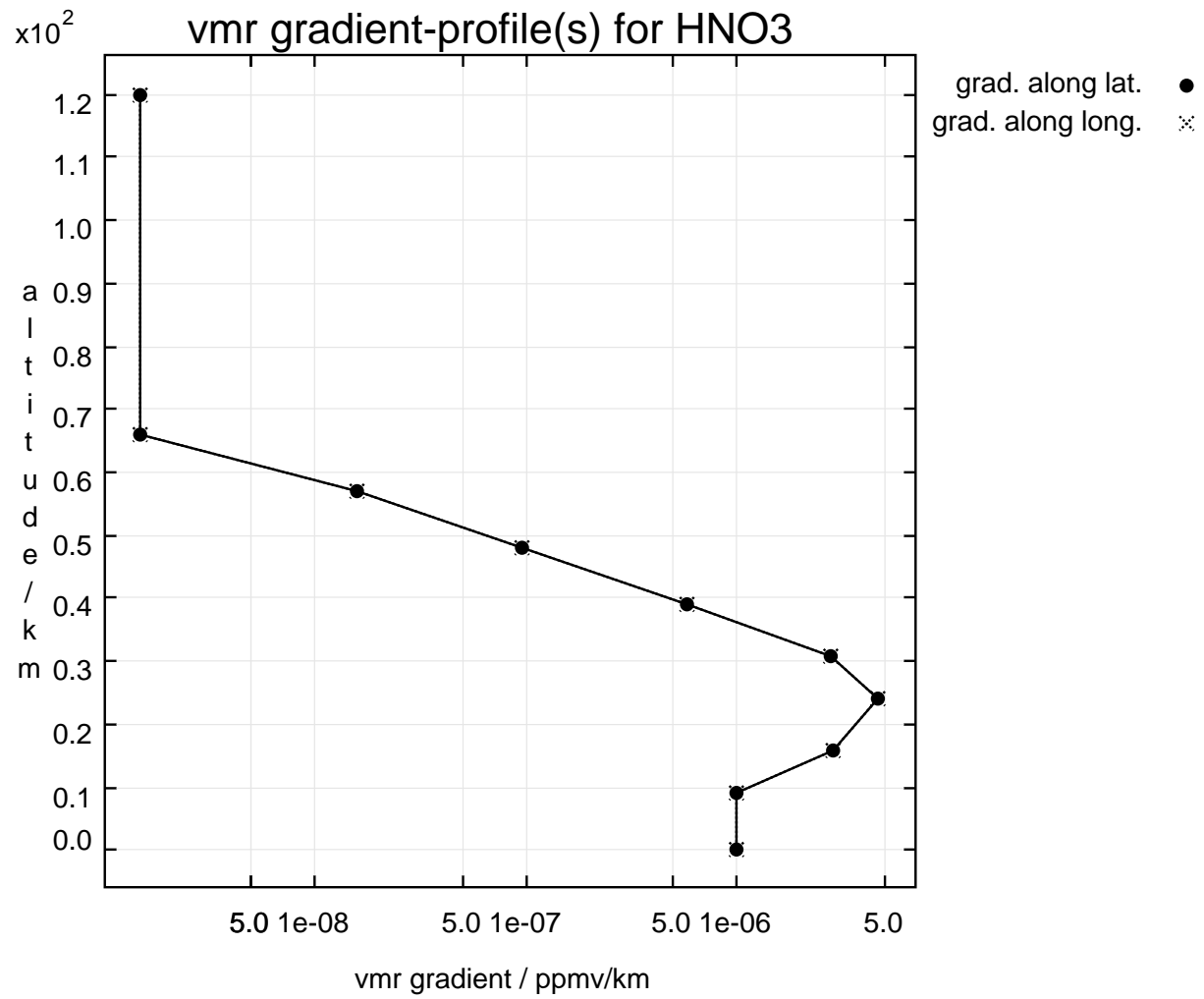


Figure 3: Horizontal inhomogeneities for O₃

Figure 4: Horizontal inhomogeneities for HNO₃

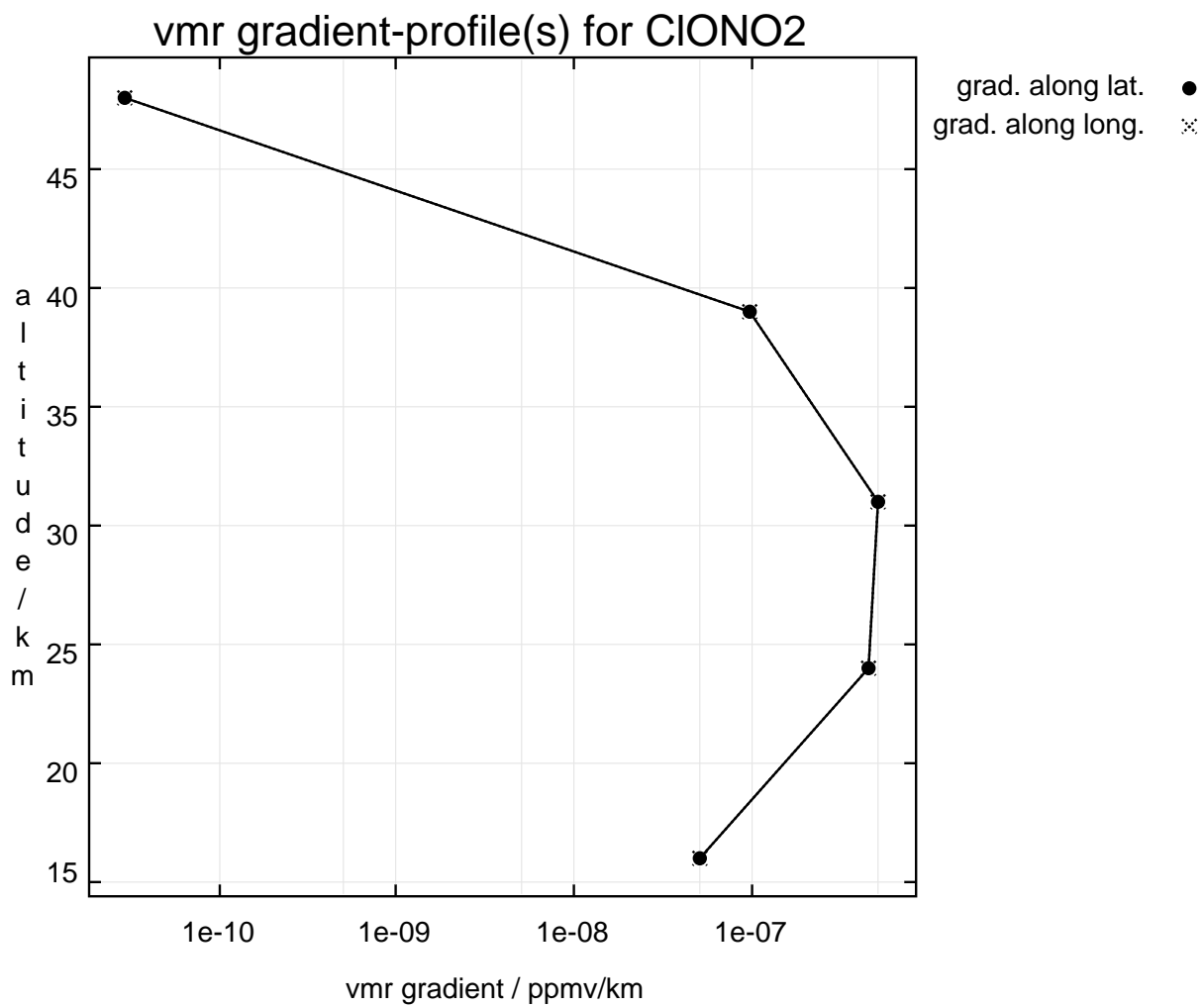
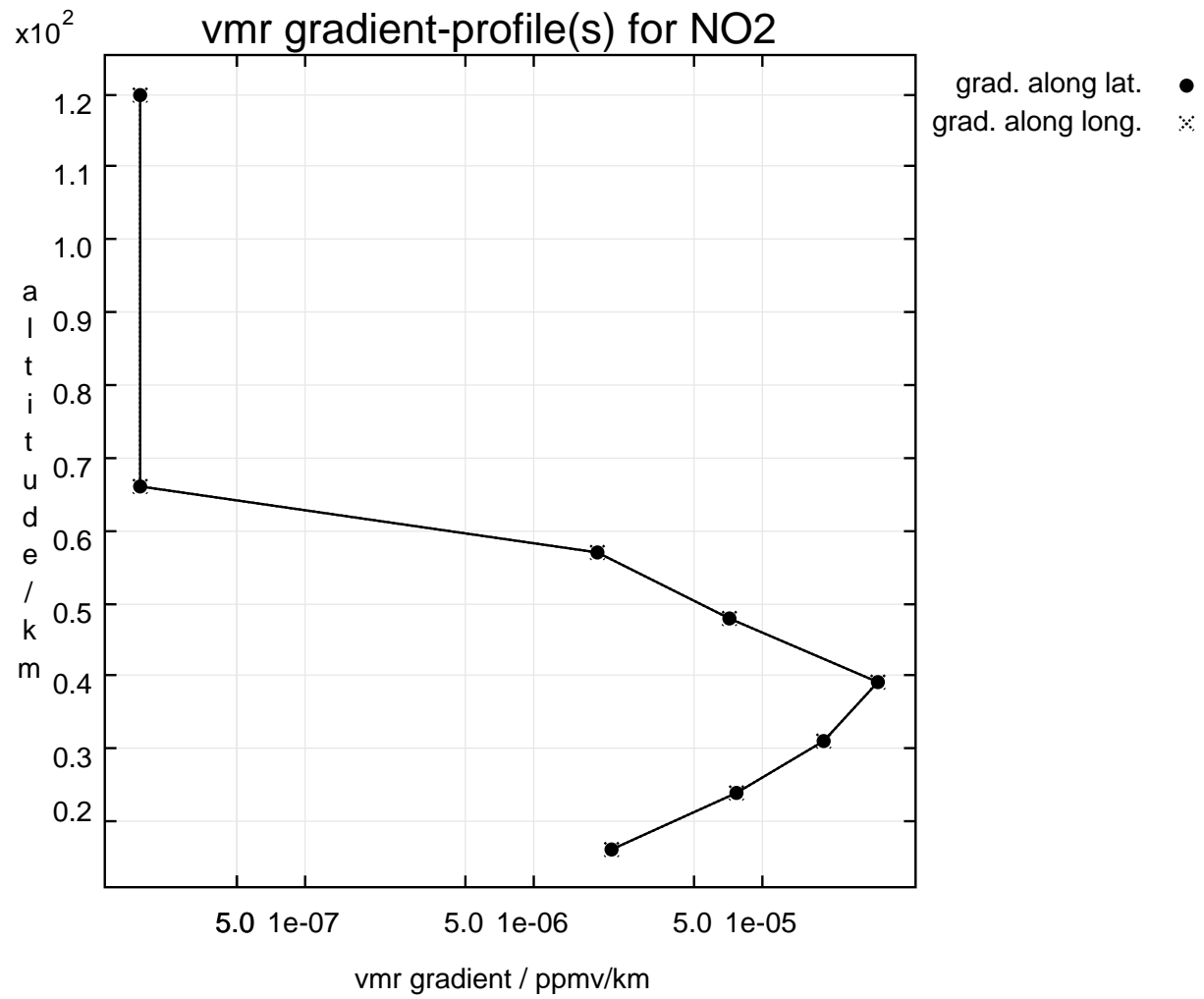


Figure 5: Horizontal inhomogeneities for ClONO₂

Figure 6: Horizontal inhomogeneities for NO₂

3.2.1 CCl₄ microwindow, 790.0 - 800.0 cm⁻¹

For this microwindow, transitions of the species H₂O, CO₂, O₃, NO₂, NH₃, HNO₃, ClO, HCN, C₂H₂, C₂H₆, COF₂, ClONO₂, and CFC-22 were taken into account, besides the target species CCl₄. The microwindow was selected to demonstrate the effect of neglecting CO₂ Q-branch line-mixing on the retrieval error, as the 791 cm⁻¹ Q-branch of the 11101 ← 10002 CO₂ transition is located on top of the CCl₄ signature. Retrieval is possible for tangent heights in the upper troposphere and lower-most stratosphere only, due to the strong decrease of CCl₄ vmr with altitude. Besides the dominating effect of line mixing, disregarding of horizontal temperature and vmr gradients, FOV and NLTE turned out to be relevant error sources. The random error of 2.6 % in 8 km tangent height is increased to a total error of 91.6 % by the errors through imperfect modeling. Spectra demonstrating the effects of disregarding the respective parameters are shown in Fig. 8 to Fig. 12, while Fig. 7 demonstrates for comparison the effect of an 5 % increase of CCl₄ vmr in the tangent layer.

3.2.2 H₂O microwindow, 1861.3 - 1861.9 cm⁻¹

This microwindow was selected as being suitable for retrieval of upper stratospheric water vapor. It contains transitions of H₂O, CO₂, O₃, N₂O, CH₄, NO and NH₃. NLTE effects were considered for H₂O, CO₂, O₃, N₂O and NO. We investigated the effects of neglecting line mixing, NLTE, temperature and pressure gradients, isotopomeric abundances, and the FOV and ILS modeling. The retrieval error for H₂O in 50 km tangent height from this microwindow is dominated by noise (35.7 %). Systematic errors contribute only to a minor extent by adding another 1 % to the over-all error budget. However, in a climatological analysis the random error will be reduced, and systematic errors can become predominant.

3.2.3 HNO₃ microwindow, 870.875 - 871.975 cm⁻¹

The microwindow selected here is suitable for retrieving HNO₃ in the lower stratosphere. It contains transitions of H₂O, CO₂, O₃, NO₂, OCS, C₂H₆, ClO, NH₃ and CFC-12. The retrieval error due to noise is assessed to be 6.7 % for 22 km tangent altitude. It is increased to 8.9 % by systematic error contributions of the horizontal inhomogeneities (vmr, temperature and pressure) and the disregarded FOV.

3.3 Conclusions

KOPRA is a powerful tool for modeling radiance and transmittance spectra as well as spatial derivatives of spectral radiances with respect to atmospheric state parameters and instrument parameters. For some typical examples, we demonstrated that the physical and instrumental modeling implemented in KOPRA is of relevance for realistic simulation of the atmospheric radiance and thus for correct retrieval results. Moreover, it must be kept in mind that modeling errors through neglection of such effects are systematic and thus may become a dominant source of retrieval error in case of temporal or spatial averaging of results where measurement noise is largely reduced. Therefore we consider the full treatment of atmospheric physics as implemented in KOPRA relevant and justified, at least for reference purposes in the context of dedicated scientific studies.

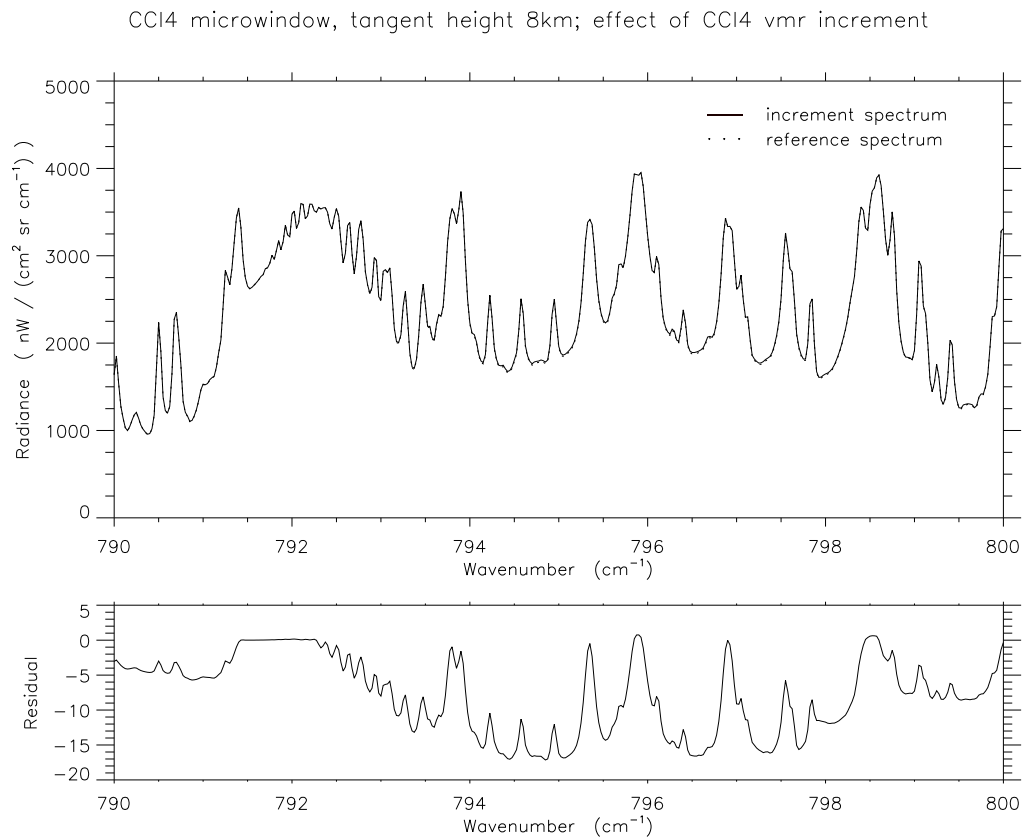


Figure 7: Spectrum of CCl₄ microwindow, tangent height 8 km: Effect of 5 % increase of CCl₄ vmr over 3 km in the tangent layer.

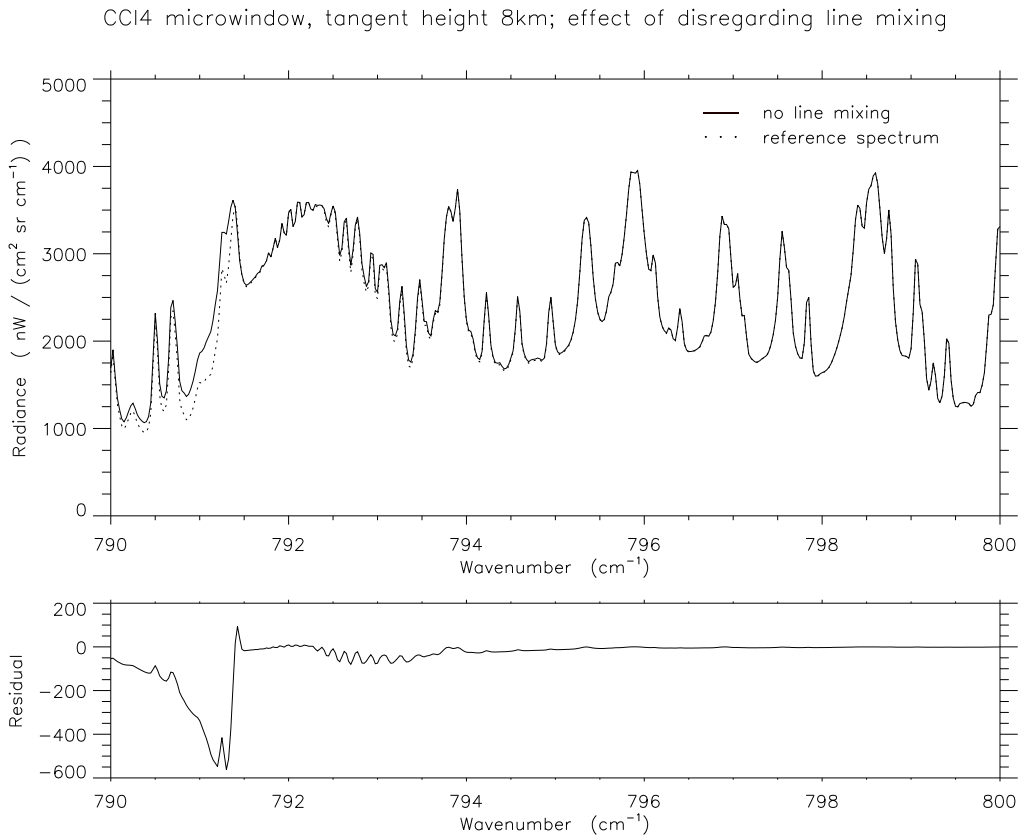


Figure 8: Spectrum of CCl₄ microwindow, tangent height 8 km: Effect of disregarding CO₂ Q-branch line mixing.

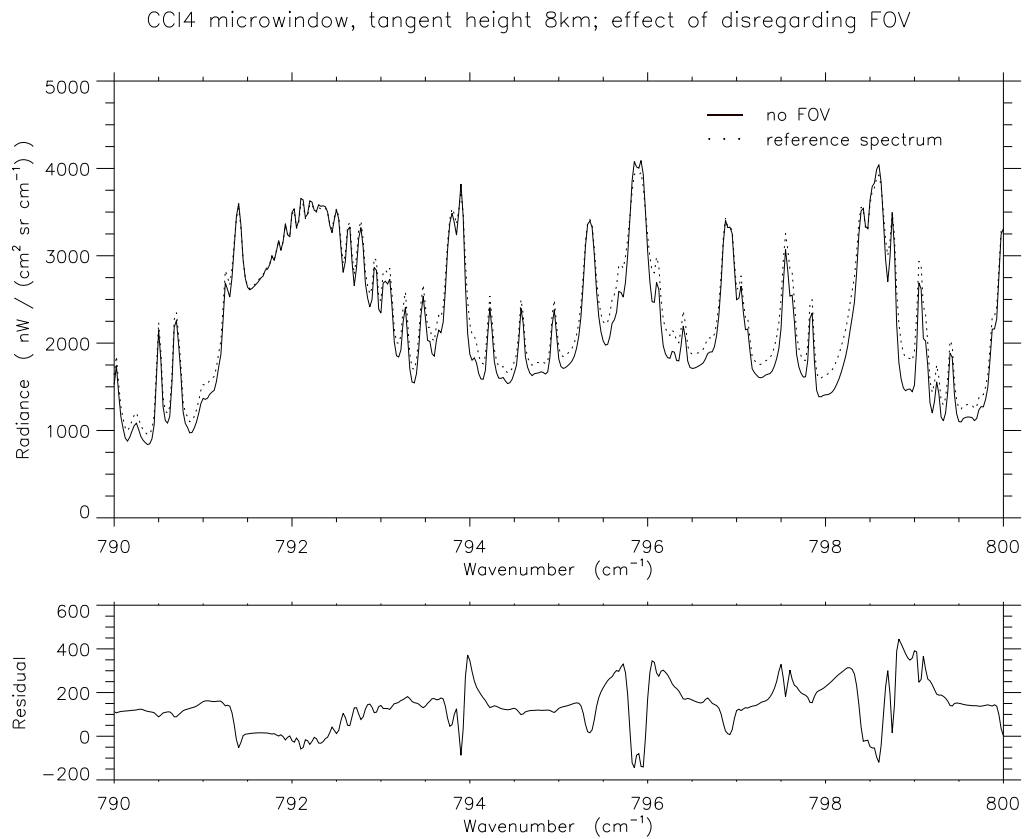


Figure 9: Spectrum of CCl₄ microwindow, tangent height 8 km: Effect of disregarding FOV modeling.

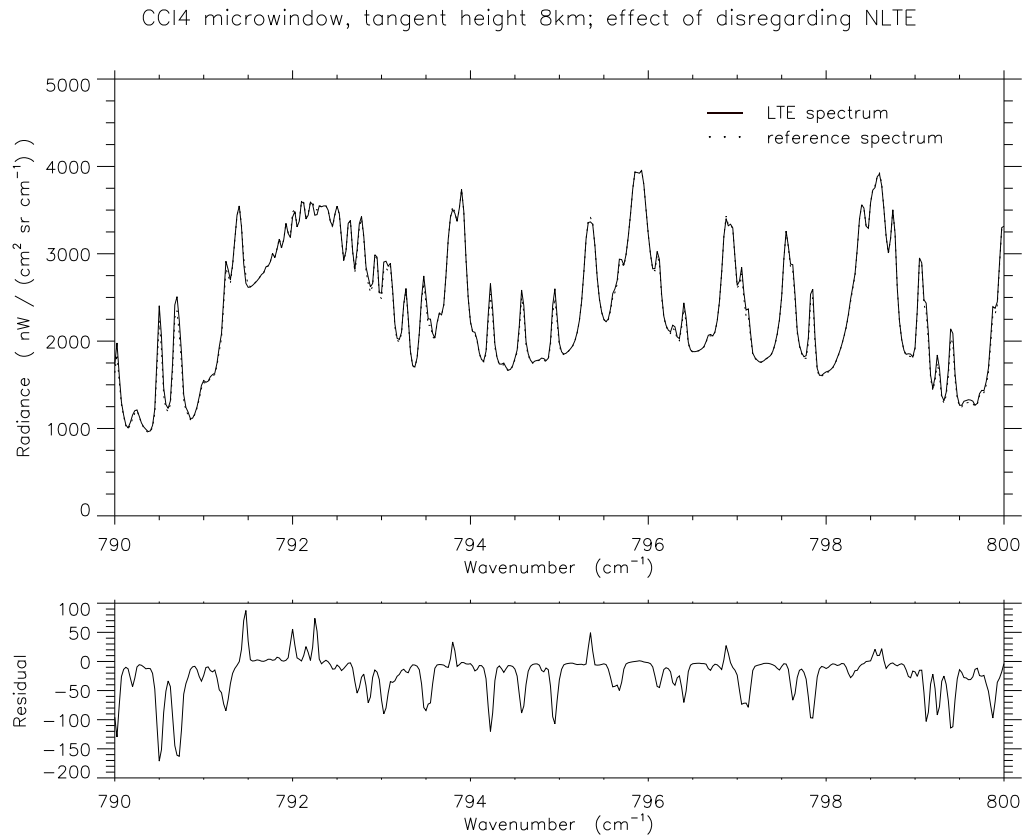


Figure 10: Spectrum of CCl₄ microwindow, tangent height 8 km: Effect of disregarding NLTE modeling.

CCl₄ microwindow tangent height 8km; effect of disregarding horizontal temperature gradients

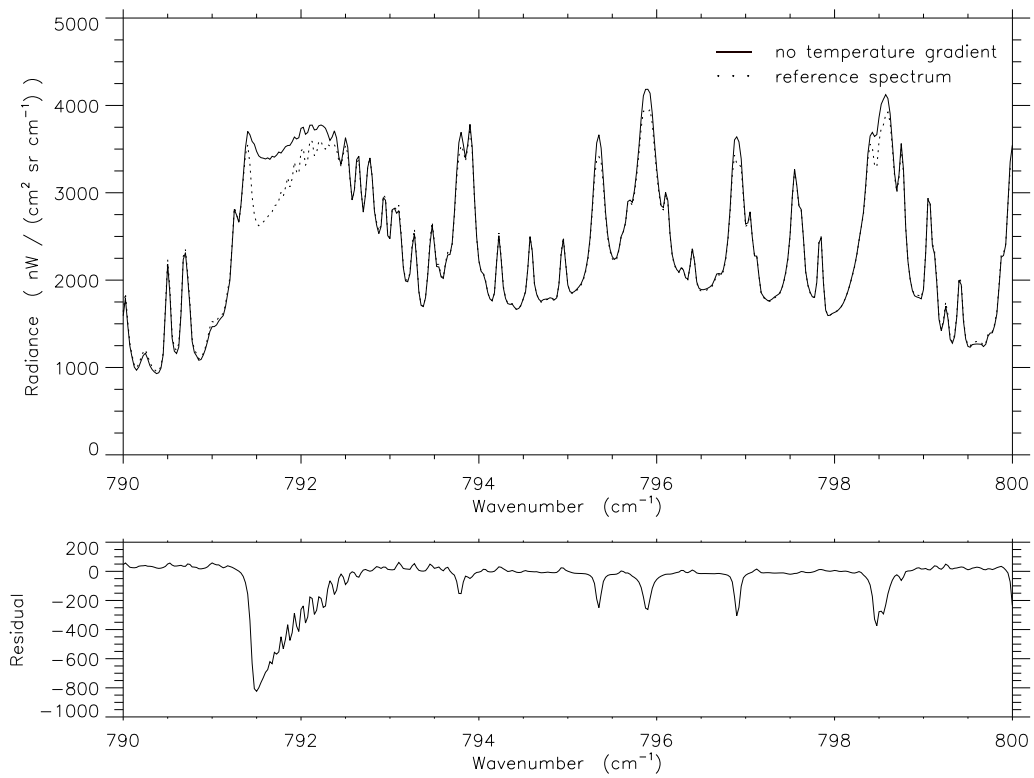


Figure 11: Spectrum of CCl₄ microwindow, tangent height 8 km: Effect of disregarding horizontal temperature gradients.

CCl₄ microwindow, tangent height 8km; effect of disregarding horizontal vmr gradients

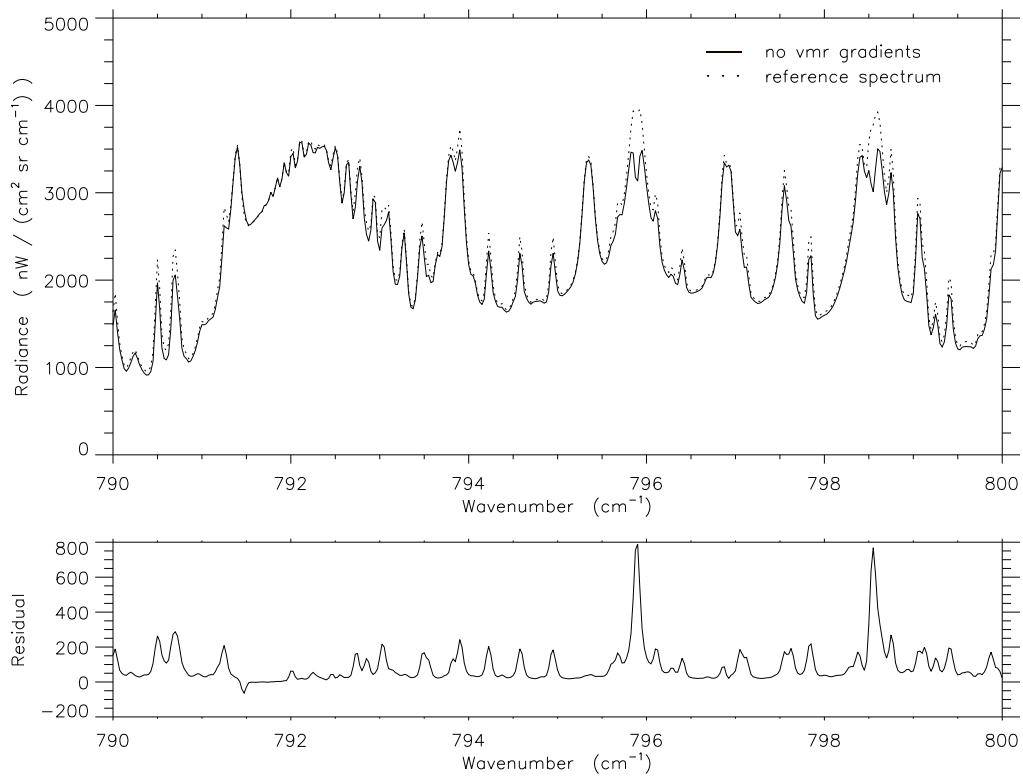


Figure 12: Spectrum of CCl₄ microwindow, tangent height 8 km: Effect of disregarding horizontal vmr gradients.

Bibliography

- [1] F. Hase and M. Höpfner, “Atmospheric ray path modeling for radiative transfer algorithms,” *Appl. Opt.* **38**(15), pp. 3129–3133, 1999.
- [2] T. von Clarmann and G. Echle, “Selection of optimized microwindows for atmospheric spectroscopy,” *Appl. Opt.* **37**(33), pp. 7661–7669, 1998.
- [3] C. D. Rodgers, “Information content and optimisation of high spectral resolution measurements,” in *Optical and Spectroscopic Techniques and Instrumentation for Atmospheric and Space Research II*, P. B. Hays and J. Wang, eds., *SPIE* **2830**, pp. 136–147, 1996.
- [4] M. Höpfner, G. P. Stiller, M. Kuntz, T. von Clarmann, G. Echle, B. Funke, N. Glatthor, F. Hase, H. Kemnitz, and S. Zorn, “The Karlsruhe optimized and precise radiative transfer algorithm. Part II: Interface to retrieval applications,” in *Optical Remote Sensing of the Atmosphere and Clouds, Beijing, China, 15–17 September 1998*, J. Wang, B. Wu, T. Ogawa, and Z. Guan, eds., *Proc. SPIE* **3501**, pp. 186–195, 1998.
- [5] T. von Clarmann, A. Dudhia, G. Echle, J.-M. Flaud, C. Harrold, B. Kerridge, A. Koutoulaki, A. Linden, M. López-Puertas, M. Á. López-Valverde, F. J. Martín-Torres, J. Reburn, J. Remedios, C. D. Rodgers, R. Siddans, R. J. Wells, and G. Zaragoza, “Study on the simulation of atmospheric infrared spectra,” tech. rep., European Space Agency, 1998. Final Report of ESA Contract 12054/96/NL/CN.
- [6] H. Nett and M. Endemann, 1996. note of June 24.
- [7] *U.S. Standard Atmosphere*, 1976. NOAA-S/T 76–1562, 10.
- [8] G. Echle, H. Oelhaf, and A. Wegner, “Measurement of atmospheric parameters with MIPAS,” tech. rep., European Space Agency, December 1992. Final Report of ESA Contract 9597/91/NL/SF.
- [9] B. Funke and M. López-Puertas, “Nonlocal thermodynamic equilibrium vibrational, rotational, and spin state distribution of $\text{NO}(\nu=0,1,2)$ under quiescent atmospheric conditions,” *J. Geophys. Res.* **105**(D4), pp. 4409–4426, 2000.
- [10] A. Dudhia, “Assessment of horizontal inhomogeneities,” tech. rep., Oxford University, October, 6 1997. Task Report on Task 2.3 of ESA Contract 12055/96/NL/CN.
- [11] B. M. Dinelli, B. Carli, and M. Carlotti, “Measurement of stratospheric distributions of H_2^{16}O , H_2^{18}O , H_2^{17}O , and HD^{16}O from far infrared spectra,” *J. Geophys. Res.* **96**(D4), pp. 7509–7514, 1991.

- [12] F. W. Irion, M. R. Gunson, C. P. Rinsland, Y. L. Yung, M. C. Abrams, A. Y. Chang, and A. Goldman, "Heavy ozone enrichments from ATMOS infrared solar spectra," *Geophys. Res. Lett.* **23**(17), pp. 2377–2380, 1996.

